# OMAE2009-79596

## Numerical Simulations of Tsunami Wave Generation by Submarine and Aerial Landslides Using RANS and SPH Models

**Kaushik Das, Ron Janetzke, Debashis Basu, Steve Green,**
**John Stamatakos**
Southwest Research Institute®
6220 Culebra Road, San Antonio, TX 78238, USA

### ABSTRACT

Tsunami wave generation by submarine and aerial landslides is examined in this paper. Two different two-dimensional numerical methods have been used to simulate the time histories of fluid motion, free surface deformation, shoreline movement, and wave runup from tsunami waves generated by aerial and submarine landslides. The first approach is based on the Navier-Stokes equation and the volume of fluid (VOF) method: the Reynolds Averaged Navier-Stokes (RANS)-based turbulence model simulates turbulence, and the VOF method tracks the free surface locations. The second method uses Smoothed Particle Hydrodynamics (SPH)—a numerical model based on a fully Lagrangian approach. In the current work, two-dimensional numerical simulations are carried out for a freely falling wedge representing the landslide and subsequent wave generations. Numerical simulations for the landslide-driven tsunami waves have been performed with different values of landslide material densities. Numerical results obtained from both approaches are compared with experimental data. Simulated results for both aerial and submerged landslides show the complex flow patterns in terms of the velocity field, shoreline evolution, and free-surface profiles. Flows are found to be strongly transient, rotational, and turbulent. Predicted numerical results for time histories of free-surface fluctuations and the runup/rundown at various locations are in good agreement with the available experimental data. The similarity and discrepancy between the solutions obtained by the two approaches are explored and discussed.

## 1. INTRODUCTION

Tsunamis are typically generated by co-seismic sea bottom displacement due to earthquakes. However, submarine or aerial landslides can trigger devastating tsunamis. Underwater landslides represent the second most important source of tsunami generation and create more devastating tsunamis than co-seismic tsunami sources of moderate strength. These types of tsunamis can produce large runup heights that flood the coast [1]. While the mechanisms that generate these types of tsunami flows are generally understood, the ability to predict the flows they produce at coastlines still represents a formidable challenge due to the complexities of coastline formations and the presence of numerous coastal structures that interact and alter the flow. Tsunami hazards posed by submarine landslides depend on the landslide scale, location, type, and process. Even small submarine landslides can be dangerous when they occur in coastal areas. Examples include the 1996 Finneidfjord slide [2] and the 1929 Grand Banks earthquake that resulted in submarine landslides, turbidity current, and a tsunami that caused significant casualties [3, 1, 4].

Although the generation and propagation of earthquake-generated tsunamis have been

studied for the last four decades and are now relatively well understood, the causes and effects of landslide-generated tsunamis are much less known. The generation and effects of landslide-generated tsunamis are complex and variable. Historical landslide-generated tsunamis have produced locally extreme wave heights of hundreds of meters, as exemplified by the greater than 100-foot wave heights in Lituya Bay, Alaska, that were generated by the 1958 Lituya Bay landslide [5].

Theoretical approaches for solving the landslide-generated tsunami problems are extremely difficult to apply due to strong nonlinearities of tsunamis, the three-dimensionality of the flow, and the turbulence that develops from a breaking tsunami. Depth averaged techniques, including Boussinesq models [6], do not predict the flowfield details accurately. Recent advances in computational fluid dynamics (CFD) have made it possible to use CFD techniques for investigation of tsunami runup. However, three-dimensional simulations of tsunami wave propagation are very difficult due to the complexity, the physical scales of the flow regimes, and the presence of the free surface. Grilli, et al. [7] used three-dimensional boundary element numerical models to predict the initial propagation of the surface disturbance. Conventionally, the Eulerian formulation is widely used to simulate tsunami flows, because it is relatively easy to implement the conservation laws of motion. Prior simulations of landslide-generated tsunamis [8-11] used models based on Navier-Stokes equations. These analyses [8-11] either used two-dimensional Navier-Stokes simulations with a VOF-type free surface tracking or a multi-fluid finite element-based Navier-Stokes model [11] in which air and water motion were simulated. Most of the simulations were carried out in a two-dimensional framework; the results were quite promising, but a full three-dimensional Navier-Stokes analysis [12, 13] was computationally very expensive. Liu, et al. [14] used a Eulerian grid-based Large Eddy Simulation (LES) technique to study the waves and runup/rundown generated by three-dimensional sliding mass. Christensen and Deigaard [15] and Lin and Liu [16, 17] used RANS models to simulate breaking waves in a surf zone. They [16, 17] used the k-ε nonlinear eddy viscosity closure model to simulate turbulence and the VOF method to track free surface locations.

RANS based approaches for simulating tsunami generation and wave propagation are computationally much more expensive than the potential flow based boundary integral equation approach. However, the RANS approach is capable of simulating the turbulence effects in tsunami wave generation and propagation. The absence of turbulence models is a deficiency of the potential flow based boundary integral equation method. However, problems of numerical diffusion in the advection terms are a complicated issue in Navier-Stokes equations. In addition, when the deformation of the free surface is very large, the numerical diffusion poses great challenge in capturing the surface accurately. In addition, the treatment of the solid material increases the complexity in these RANS based approaches of tsunami modeling.

Another class of numerical methods is based on the Lagrangian formulation. Several Lagrangian formulations based on meshfree methods have been proposed in recent years, including SPH and the Lattice Boltzmann Method (LBM) [18]. Of the different techniques developed over the past decade, SPH has been the most popular and successful when applied to free-surface hydrodynamics. SPH, a fully Lagrangian approach, was originally developed to simulate non-axisymmetric problems in astrophysics that predict the motion of discrete particles with time. SPH obtains approximate numerical solutions of the equations of fluid dynamics by replacing the fluid with a set of points. Using a kernel function, these points can be used to discretize partial differential equations of fluid dynamics without any underlying mesh. The basic theory of SPH is based on the discrete summation over disordered points as an approximation to integrals. One of the major advantages of SPH is that the need for fixed computational grids is removed when calculating spatial derivatives. Since its initial development by Gingold and Monaghan [19] and Lucy [20], the technique has been applied to many other problems including free-surface hydrodynamics [18, 21, and 22], fracture problems [18], and impact modeling [18]. SPH techniques have been successfully applied for simulating water waves [21-24]. Liu and Liu [18] have provided a very good description of the meshfree SPH method in simulating a wide range of fluid dynamics problems. Due to its ability to effectively simulate complex fluid structure interaction problems involved in wave impacts and wave sloshing, the SPH method is a viable and attractive alternative for simulating tsunami

propagation problems. However, there are some inherent problems in SPH related to implementation of boundary conditions on fluid-solid surface. In addition, the numerical stability of the SPH method is determined by the kernel function and particle smoothing length.

In the present work, both the Navier-Stokes equations as well as the SPH model [24] are used to predict the aerial and submerged landslide movement and the subsequent generation and propagation of tsunami waves. The two approaches are assessed in terms of their relative advantages and disadvantages for simulation of tsunami generation and propagations. Two-dimensional simulations are carried out for the Navier-Stokes equations; the flow solver FLOW-3D [25] is used. The VOF method is used in FLOW-3D to track the free surface and shoreline movement. Turbulence in the Navier-Stokes equations is simulated using the renormalization group (RNG)-based turbulence model [26]. For the SPH simulations, the baseline SPH code provided by Liu and Liu [24] was modified for the current applications. Numerical results from the simulations are compared with experimental data [27, 14]. The two approaches are compared for the tsunami wave generation by aerial and submarine landslides. The predicted solution by the Navier-Stokes equations and preliminary results from the SPH simulations are compared with the available experimental data [27, 14] for the time histories of free-surface fluctuations and the runup/rundown at various locations.

## 2. NAVIER-STOKES SOLVER METHODOLOGY

FLOW-3D [25], developed by Flow Sciences, is a general purpose CFD simulation software package based on the algorithms for simulating fluid flow that were developed at Los Alamos National Laboratory in the 1960s and 1970s [28-30]. The basis of the solver is a finite volume or finite difference formulation, in Eulerian framework, of the equations describing the conservation of mass, momentum, and energy in a fluid. The code is capable of simulating two-fluid problems, incompressible and compressible flow, and laminar and turbulent flows. The code has many auxiliary models for simulating phase change, non-Newtonian fluids, non-inertial reference frames, porous media flows, surface tension effects, and thermo-elastic behavior. FLOW-3D solves the fully three-dimensional transient Navier-Stokes equations using the Fractional Area/Volume Obstacle Representation (FAVOR) [31] and the volume of fraction [28] method. The solver uses finite difference or finite volume approximation to discretize the computational domain. Most of the terms in the equations are evaluated using the current time-level values of the local variables in an explicit fashion, though a number of implicit options are available. The pressure and velocity are coupled implicitly by using the time-advanced pressures in the momentum equations and the time-advanced velocities in the continuity equations. It solves these semi-implicit equations iteratively using relaxation techniques. FAVOR [31] defines solid boundaries within the Eulerian grid and determines fractions of areas and volumes (open to flow) in partially blocked volume to compute flows correspondent to those boundaries. In this way, boundaries and obstacles are defined independently of grid generation, avoiding saw-tooth representation or the use of body-fitted grids. FLOW-3D has a variety of turbulence models for simulating turbulent flows, including the Prandtl mixing length model, one-equation model and two-equation k-ε model, RNG scheme, and an LES model. The current simulations use the RNG model [26].

## 3. RNG TURBULENCE MODEL

The RNG turbulence model [26] solves for the turbulent kinetic energy (k) and the turbulent kinetic energy dissipation rate (ε). This RNG approach applies statistical methods to derive the averaged equations for turbulent quantities, such as turbulent kinetic energy (k) and its dissipation rate. The RNG-based models rely less on empirical constants while setting a framework for the derivation of a range of parameters to be used at different turbulence scales. The RNG model uses equations similar to those for the k-ε model. However, equation constants that are found empirically in the standard k-ε model are derived explicitly in the RNG model. Generally, the model has wider applicability than the standard k-ε one.

## 4. SMOOTHED PARTICLE HYDRODYNAMICS

The SPH model is based on two fundamental ideas: every flow characteristic is smoothed over the spatial domain by using an appropriate kernel function and the smoothed flow is approximated by particles, whose time evolution is governed by a Lagrangian scheme [32]. There are no constraints imposed on the geometry of the system or on how far it may evolve from the initial conditions. The SPH

equations are obtained from the continuum equations of fluid dynamics by interpolating from a set of points that may be disordered. The interpolation is based on the theory of integral interpolants using interpolation kernels, which approximate a delta function. The interpolants are analytic functions, which can be differentiated without the use of grids. The gradient and divergence terms in the fluid dynamical equations can therefore be obtained from information at neighboring points, which can be thought of as particles. As a consequence, the equations of fluid dynamics reduce to a set of ordinary differential equations for the motion of each particle. The simulation of a fluid then becomes an n-body problem with the interactions between the particles determining how their properties change. In the SPH numerical implementation, the fluid domain is represented by a certain finite number of particles, carrying the physical variable at the points occupied by their volumes. SPH enables the user to perform computation with any arbitrary distribution of particles and deal with extremely large deformation [33-35]. The SPH formulation used in the code is detailed in references 24, 33, and 34 and is not described in this paper. The artificial viscosity used in the code is based on Monaghan's formula [34], and Batchelor's formula [36] has been used for the relationship between pressure and density. The boundary condition based on the repulsive force as given by Monaghan [23, 34] is used in the current simulations.

### 5. EXPERIMENT

Two sets of simulations were carried out in the present work. They are the sliding wedge wave tank experiment at Oregon State University [14] and the experiment involving wave generation by a rigid wedge sliding into water along an incline by Heinrich [27]. The first experiment on the sliding wedge wave tank was conducted at Oregon State University. The wave tank has a length of 104 m, a width of 3.7 m, and a depth of 4.6 m. A plane slope (a beach with an inclination of two horizontal to one vertical) was located near one end of the tank and a dissipating beach at the other end. For all experiments, the water depth in the wave tank was about 2.44 m. The landslide was represented by a sliding wedge. The sliding wedge moved down the slope by gravity, rolling on specially designed v-shaped wheels (with low friction bearings) that ride on aluminum strips with shallow grooves

inset into the slope. Figure 1 shows the schematic sketch of the experiment and the nomenclature used in the experiments. The length of the wedge (b) is 91.44 cm; a front face dimension (a) is 45.72 cm high. In Figure 3, the distance, x, is measured seaward from the intersection of the seawater level (SWL) with the slope. The runup, R, is measured vertically from the SWL, and $\Delta$ is the vertical distance from the SWL to the highest point measured positively upward from the SWL. In the experiment, a sufficient number of wave gauges were used to determine the seaward-propagating waves (the waves propagating to either side of the sliding bodies).

The second experiment was by Heinrich [27]. The experiments were carried out in a channel that was 20-m long, 0.55 m wide, and 1.50 m deep in the Hydraulic National Laboratory, Chatou, France [27]. In this experiment, water waves were generated by allowing a wedge to freely slide down a plane inclined at $45°$ on the horizontal. The wedge was triangular in cross section (0.5 m × 0.5 m) with a 2000 kg/m$^3$ density. The water depth was 1 m and the top of the edge was initially 1 cm below the horizontal free surface. The box was equipped with four rollers, slid into the water under the influence of gravity only, and was abruptly stopped as it reached the bottom by a 5-cm-high rubber buffer. The box was held in its initial position by a hydraulic jack moving laterally through the unglazed side wall [27]. The experimental setup [27] is shown in Figure 2.

### 6. COMPUTATIONAL DETAILS

The Navier-Stokes solutions were obtained with FLOW-3D. Figure 3 shows the computational domain and grid for the simulations with the Oregon State University experimental configuration [14]. A two-dimensional flow domain representing the experiment setup Liu, et al. [14] described was defined within the framework of the FLOW-3D software. The entire flow domain is 100 m in length and 5.6 m in height. The flow domain near the ramp is detailed in Figure 3. The ramp in these experiments has a 1:2 slope, and the wedge is placed so that its leading edge is initially at the undisturbed water surface. The water depth is specified as 4.6 m and the ramp is 10.114 m down the length of the flow domain. The sliding block is about 0.457 m in height and 0.914 m in length.

The computational grid for these simulations consisted of 400 × 56 grids in the x and y directions, respectively. The grid is nearly uniform in the region covering the ramp, and the x-grid expands from the end of the ramp to the end of the flow channel. The grid also covers the initial air space above the water to accommodate the block motion and the surface waves. This feature is required in the FLOW-3D software as part of its VOF free-surface tracking algorithm. All surfaces of the flow domain were defined as no-slip smooth walls. Similarly, the faces of the wedge and ramp were also smooth no-slip surfaces. The wedge motion is specified as a constant 2.9 m/s down the ramp consistent with the average velocity of the wedge in one of the test runs Liu, et al. [14] described. The fluid in the channel was specified as water with a density of 1000 kg/m$^3$ and a viscosity of 1 cP. In the experiments Liu, et al. [14] described, air filled the space above the water. In these current simulations, however, this was empty space that did not interact with the water. First a laminar-only condition for the entire flowfield was used. Second, an RNG turbulence model was used to capture any turbulence effects near the moving wedge.

Figure 4 shows the computational domain and grid for the simulations with the experimental data of Heinrich [27]. A two-dimensional flow domain representing the experiment setup described was defined within the framework of the FLOW-3D software. The entire flow domain, Figure 6, is 4.1 m in length and 1.2 m in height. The ramp in these experiments has a 1:1 slope, and the wedge is placed so that its top face is submerged 0.1 m below the water surface. The water depth is specified as 1.0 m. The coordinate system for these simulations has its origin at the bottom of the flow channel directly below the location where the water surface meets the boundary. The computational grid comprises a uniform grid of 120 × 40 cells in the x and z directions, respectively. Note that the grid also covers the initial air space above the water to accommodate the block motion and the surface waves as required in the FLOW-3D software as part of its VOF free-surface tracking algorithm. All surfaces of the flow domain were defined as no-slip smooth walls. Similarly, the faces of the wedge and ramp were also smooth no-slip surfaces. The wedge motion follows the prescribed velocity profile Ashtiani, et al. [37] specified. This velocity profile is a piecewise linear fit to the following function

$$V(t)=86\tanh(0.0175t), \quad t \leq 0.4s \qquad (1)$$
$$V(t)=0.6 \qquad\qquad t > 0.4s \qquad (2)$$

where the velocity units are m/s. The prescribed time history of the wedge speed is described in Figure 5. Note that the velocity profile is very nearly linear during the block acceleration. In these simulations, the block was decelerated to a stop between t=1.4 s and t=1.45 s so that it rested at the bottom of the ramp. The fluid in the channel was specified as water with a density of 1000 kg/m$^3$ and a viscosity of 1 cP. In the experiments described [27, 37], air filled the space above the water. In these simulations, however, this was empty space that did not interact with the water. Laminar flow conditions prevail over most of the flow domain except near the moving edge. Consequently, two scenarios were simulated. Turbulence was simulated using the RNG turbulence model to capture any turbulence effects near the moving wedge.

The SPH simulations used the same experimental configuration and geometry [14, 27]. The simulations for the experimental configuration of Heinrich [27] used 3000 particles, which included 2500 fluid particles and 500 boundary particles. The computational domain had a vertical wall on the right at 4 m on the X axis and a 45.0° floor sloping from 2 m height at −1.0 m on the Y axis to 0.0 m height at 1.0 m on the X axis. A movable 0.5 m × 0.5 m wedge was placed on the sloping floor with a horizontal face on top and the vertical face on the right, which was positioned at 0.5 m on the X axis. The wedge was placed at 1 m, which was also the free surface height of the water. The wedge started to move at 0.1 s and stopped at the bottom of the tank at 1.5 s. The simulations used a constant time step of 0.001 s.

The SPH simulations for the experimental configuration of Oregon State University and Liu, et al. [14] used 15000 particles. That included 13500 fluid particles and 1500 boundary particles. The computational domain consisted of a vertical wall on the right at 20 m on the X axis and a floor with a 2:1 slope and 4.5 m height. The setup included a movable 1.0 by 0.5 m wedge placed on the sloping floor with a horizontal face on top and the vertical face on the right. This placed the top of the wedge at 2.95 m. The water height was 2.45 m, with the bottom of the tank at 0.0 m on the Y axis. The wedge started to move at 0.1 s and stopped at the bottom of the tank at 2.5 s. The simulations for the experimental configuration of Oregon State

University and used a constant time step of 0.001 s. The repulsive boundary condition of Monaghan [22] was used for the wall boundary condition.

## 7. RESULTS AND DISCUSSIONS

Computational results are presented for the Navier-Stokes simulations and the SPH simulations of the two experimental configurations [14, 27]. Presented results include the unsteady fluid configurations at different times and comparison of the predicted water surface height and elevation with experimental observations.

Figures 6 through 10 present computational results for the Heinrich [27] simulations. Figure 6 present fluid configurations at different times. The initial wave is shown at time t=0.6 s, when the trough behind the wave is about at its minimum position. The fluid configuration at 1.2 s shows that the second wave is just being formed as a result of the continued wedge motion and the reflection of the back of the initial wave from the ramp. Finally, at time t=1.8 s, the second wave is seen to be propagating down the channel just above the block. Note that the vortex initially behind the top corner of the block has detached from the block by time t=1.8 s.

The experimental and simulated wave profiles are compared in Figure 7. The fluid surface shape for times t=0.5 s and t=1.0 s are shown in Figure 7. At time t=0.5 s, the latter half of the wedge is just beginning to be covered by fluid as the initial wave is generated. At t=1.0 s, the wave is running up on the ramp behind the wedge. Simulated results closely agree with the experimental observation [27].

Figure 8 shows the initial fluid configuration for the SPH simulations with the configuration of Heinrich [27]. Figure 9 presents the particle configuration due to the wedge movement at different times from the SPH simulations. Close agreement can be seen between the water surface elevation obtained from the Navier-Stokes simulations (Figure 6) and the SPH results. Simulated SPH results show the generation of waves and their reflection from the left wall. The water surface is nearly horizontal at t=1.5 seconds. It can be observed from figure 9 that at t=1 s, a vortex is being generated above the wedge, and at t=1.5 s, the wedge reaches the bottom. The formation of the vortex and the flowfield structure obtained from the SPH simulations are in good agreement with the results obtained from the Navier-Stokes

simulations. However, note that the SPH simulations did not use any turbulence model for simulating the turbulence. The general viscosity formulation of Monaghan [22] has been used for the artificial viscosity. The artificial vorticity formulation has successfully predicted the vortex structure in the flowfield.

Figure 10 shows the comparison of the water surface elevations at t=0.5 s and t=1.0 s the SPH simulations predicted with the experimental data. Note that the SPH simulations have predicted the correct trend of the water surface elevations. However, their magnitudes are overpredicted compared to the experimental results because the fact that the current simulations did not have any turbulence models. Comparing figures 7 and 10, one can see that the Navier-Stokes simulations also overpredicted the water surface elevation up to 0.75 m after which the elevation level was underpredicted. Future simulations with the SPH models will aim at evaluating the effect of turbulence models and turbulence viscosity on the solution.

Figures 11 through 15 present the results from the simulations with the experimental configuration of Oregon State University [14]. Figure 11 shows the flowfield at different time levels obtained from the Navier-Stokes solution. In all of these figures, the fluid surface and the pressure contours are shown. The pressure contours are increasing from atmospheric value at the surface to the bottom, corresponding to a value of about 45 kPa. At t=0.6 s, the initial wave is created when the wedge is just submerged. The front of this wave begins to travel downstream, and the back of the wave breaks backward over the top of the wedge. At t=1.2 s, the wave has completely broken over the wedge and begins to run up the ramp. At 2.6 s, the flow has the maximum wave runup on the ramp. A small vortex forms as the wedge slides down. At t=4.0 s, a second wave is formed and propagates down the channel.

Figure 12 shows the snapshots of velocity vectors on the centerline vertical plain for the sliding wedge from the three-dimensional LES results of Liu, et al. [14]. Comparing Figures 11 and 12, shows a qualitative agreement between the current simulations and the LES of Liu, et al. [14]. Even though the simulations by Liu, et al. [14] used LES and a much larger grid compared to the current simulations, the present simulations show good agreement with their results.

The predicted wave height from the current two-dimensional Navier-Stokes simulations is

compared to the measured wave heights and the three-dimensional numerical predictions of Liu, et al. [14] in Figure 13. Note that the wave heights the two-dimensional simulations predicted are greater than those measured in the experiments because the lateral spreading of the wave is not captured in the two-dimensional simulations. The wave frequency predicted from the two-dimensional simulations, however, is in relatively good agreement with the measurements.

Figure 14 shows the initial fluid configuration for the SPH simulations with the configuration of Liu et al. [14]. Figure 15 shows the unsteady flowfield and sequential fluid runup at different times for the SPH simulations of the configuration of Liu et al. [14]. The SPH simulations can capture the basic features of the flowfield. The SPH model has predicted the formation of the initial wave, the reflection of the wave, and subsequent runup. The formation of a vortex over the wedge as it slides down the ramp can also be observed in the figures. Comparing figures 11 and 15, the predicted wave runup is greater for the SPH simulations compared to the Navier-Stokes RANS simulations. However, there is qualitative agreement between the velocity field predicted by the RANS model and the SPH model.

## 8. CONCLUSIONS

Two two-dimensional numerical models—the Navier-Stokes RANS with a VOF free-surface method and the SPH method—have been presented for simulations of tsunami wave generation by aerial landslides. Simulations are carried out for two experimental configurations. The capability and accuracy of these models are evaluated by comparing the numerical results with available experimental data. Simulated results for both landslide configurations show the complex flow patterns in terms of the velocity field, shoreline evolution, and free-surface profiles. In general, the numerical results obtained from both the models are in reasonable agreement with the experimental data in terms of the water surface elevation and the flowfield. The RANS model appears to better predict the surface elevation profile compared to the SPH. The SPH simulations overpredict the surface elevation profiles. This can be due to the lack of sufficient diffusion in the SPH numerical scheme. The velocity fields predicted by the RANS model and the SPH model are in good qualitative agreement. The differences in prediction between the SPH and the RANS

models can be attributed to numerical resolution, numerical diffusion, and turbulence models. Future studies will provide in-depth analysis of the effect of numerical resolution, diffusion, and the turbulence model on the SPH predictions.

## 9. ACKNOWLEDGMENTS

## 10. REFERENCES

1. Masson, D. G., Harbitz, C. B., Wynn, R. B., Pedersen, G., and Lovholt, F., 2006, "Submarine Landslides: Processes, Triggers and Hazard Prediction," Philosophical Transaction of the Royal Society, Vol. 364, pp. 2009–2039.
2. Longva, O., Janbu, N., Blikra, L. H., and Boe, R., 2003, "The Finneidfjord Slide: Seafloor Failure and Slide Dynamics," Submarine Mass Movements and Their Consequences, J. Locat and J. Mienert, eds., Kluwer Academic Publishers, Dordrecht, Netherlands, pp. 531–538.
3. Fine, I. V., Rabinovich, A. B., Bornhold, B. D., Thomson, R. E., and Kulikov, E. A., 2005, "The Grand Banks Landslide-Generated Tsunami of November 18, 1929: Preliminary Analysis and Numerical Modeling," Marine Geology, Vol. 203, pp. 201–218.
4. Piper, D. J. W., Cochonat, P., and Morrison, M. L., 1999, "The Sequence of Events Around the Epicenter of the 1929 Grand Banks Earthquake: Initiation of Debris Flows and Turbidity Currents Inferred From Sidescan Sonar," Sedimentology, Vol. 46, pp. 79–97.
5. Miller, D. J., 1960, "Giant Waves in Lituya Bay, Alaska," Geological Survey Professional Paper 354-C, U.S. Government Printing Office, Washington, D.C.
6. Lynett, P., Wu, T.-R., and Liu, P. L.-F., 2002, "Modeling Wave Runup with Depth Integrated Equations," Coastal Engineering, 46(2), pp. 89–107.
7. Grilli, S. T., Vogelmann S., and Watts, P., 2002, "Development of a 3D Numerical Wave Tank for Modeling Tsunami

Generation by Underwater Landslides," Engineering Analysis with Boundary Elements, 26(4), pp. 301–313.

8. Liu, P. L.-F., Wu, T.-R., Raichlen, F., Synolakis, C. E., and Borrero, J. C., 2005, "Runup and Rundown Generated by Three-Dimensional Sliding Masses," Journal of Fluid Mechanics, Vol. 536, pp. 107–144.

9. Grilli, S. T., and Watts, P., 1999, "Modeling of Waves Generated by a Moving Submerged Body, Applications to Underwater Landslides," Engineering Analysis with Boundary Elements, Vol. 23, pp. 645–656.

10. Lynett, P., and Liu, P. L.-F., 2005, "A Numerical Study of the Runup Generated by Three-Dimensional Landslides," Journal of Geophysical Research, 110(C03006), doi:10.1029/2004JC002443.

11. Rzadkiewicz, A. S., Mariotti, C., and Heinrich, P., 1997, "Numerical Simulation of Submarine Landslides and Their Hydraulic Effects," Journal of Waterway, Port, Coastal, and Ocean Engineering, 123(4), pp. 149–157.

12. Gisler, G., Weaver, R., Mader, C., and Gittings, M. L., 2003, "Two- and Three-Dimensional Simulations of Asteroid Ocean Impacts," Science of Tsunami Hazards, 21(2), pp. 119–134.

13. Gisler, G., Weaver, R., and Gittings. M. L., 2006, "SAGE Calculations of the Tsunami Threat From La Palma," Science of Tsunami Hazards, 24(4), pp. 288–301.

14. Liu, P. L.-F., Wu, T.-R., Raichlen, F., Synolakis, C. E., and Borrero, J. C., 2005, "Runup and Rundown Generated by Three-Dimensional Sliding Masses," Journal of Fluid Mechanics, Vol. 536, pp. 107–144.

15. Christensen, E. D., and Deigaard, R., 2001, "Large Eddy Simulation of Breaking Waves," Coastal Engineering, Vol. 42, pp. 53–86.

16. Lin, P., and Liu, P. L.-F, 1998, "A Numerical Study of Breaking Waves in the Surf Zone," Journal of Fluid Mechanics, Vol. 359, pp. 239–264.

17. Lin, P., and Liu, P. L.-F, 1998, "Turbulence Transport, Vortices Dynamics, and Solute Mixing Under Plunging Breaking Waves in Surf Zone," Journal of Geophysical Research, 103(C8), pp. 15677–15694.

18. Liu, G. R., and Liu, M. B., 2003, "Smoothed Particle Hydrodynamics: A Mesh-Free Particle Method," World Scientific Publishing Company, Singapore.

19. Gingold, R. A., and Monaghan, J. J., 1977, "Smoothed Particle Hydrodynamics: Theory and Application to Non-Spherical Stars," Monthly Notices to Royal Astronomical Society, Vol. 181, pp. 375–389.

20. Lucy, L. B., 1977, "Numerical Approach to Testing the Fission Hypothesis," Astronomical Journal, Vol. 82, pp. 1013–1024.

21. Monaghan, J. J., and Kos, A., 2000, "Scott Russell's Wave Generator," Physics of Fluids, 12(3), pp. 622–630.

22. Monaghan, J. J., and Kos, A, 1999, "Solitary Waves on a Cretan Beach," Journal of Waterway, Port, Coastal, and Ocean Engineering, Vol. 145, pp. 125–131.

23. Monaghan, J., 1994, "Simulating Free Surface Flows with SPH," Journal of Computational Physics, Vol. 110, pp. 399–406.

24. Dalrymple, R. A., and Rogers, B. D., 2006, "Numerical Modeling of Water Waves with the SPH Method," Coastal Engineering, 53(2-3), pp. 141–147.

25. Flow Sciences, Incorporated, 2006, "Flow3D Users Manual Version-9.1," Flow Sciences, Incorporated, Santa Fe, New Mexico.

26. Yakhot, V., and Smith, L. M., 1992, "The Renormalization Group, the e-Expansion and Derivation of Turbulence Models," Journal of Scientific Computing, Vol. 7, pp. 35–61.

27. Heinrich, P., 1992, "Nonlinear Water Waves Generated by Submarine and Aerial Landslides," Journal of Waterway, Port, Coastal and Ocean Engineering, 118(3), pp. 249–266.

28. Hirt, C. W., and Nichols, B. D., 1981, "Volume of Fluid (VOF) Method for the Dynamics of Free Boundaries," Journal of Computational Physics, Vol. 39, pp. 201–225.

29. Harlow, F. H., and Welch, J. E., 1965, "Numerical Calculation of Time-Dependent Viscous Incompressible Flow," Physics of Fluids, Vol. 8, pp. 2182–2189.

30. Welch, J. E., Harlow, F. H., Shannon, J. P., and Daly, B. J., 1966, "The MAC Method: A Computing Technique for Solving Viscous, Incompressible, Transient Fluid Flow Problems Involving Free-surfaces," Los Alamos Scientific Laboratory Report LA-3425.

31. Hirt, C. W., and Sicilian, J. M., 1985, "A Porosity Technique for the Definition of Obstacles in Rectangular Cell Meshes," Proceedings of the Fourth International Conference on Ship Hydrodynamics, National Academy of Sciences, Washington, D.C., National Academy of Sciences, pp. 1–19.

32. Yim, S. C., Yuk, D., Panizzo, A., Di Risio, M., and Liu, P. L.-F., 2008, "Numerical Simulations of Wave Generation by a Vertical Plunger Using RANS and SPH Models," Journal of Waterway, Port, Coastal and Ocean Engineering, 134(3), pp. 143–159.

33. Monaghan, J. J., 2005, "Smoothed Particle Hydrodynamics," Reports on Progress in Physics, Vol. 68, pp. 1703–1759.

34. Monaghan, J. J., 1992, "Smoothed Particle Hydrodynamics," Annual Review of Astronomy and Astrophysics, Vol. 30, pp. 543–574.

35. Liu, M. B., Liu, G. R., Zong, Z., and Lam, K. Y., 2003, "Smoothed Particle Hydrodynamics for Numerical Simulation of Underwater Explosions," Computational Mechanics, 30(2), pp. 106–118.

36. Batchelor, G. K., 1974, "Introduction to Fluid Dynamics," Cambridge University Press, Cambridge, Massachusetts.

37. Ataie-Ashtiani, B., and Shobeyri, G., 2008, "Numerical Simulation of Landslide Impulsive Waves by Incompressible Smoothed Particle Hydrodynamics," International Journal of Numerical Methods in Fluids, Vol. 56, pp. 209–232.
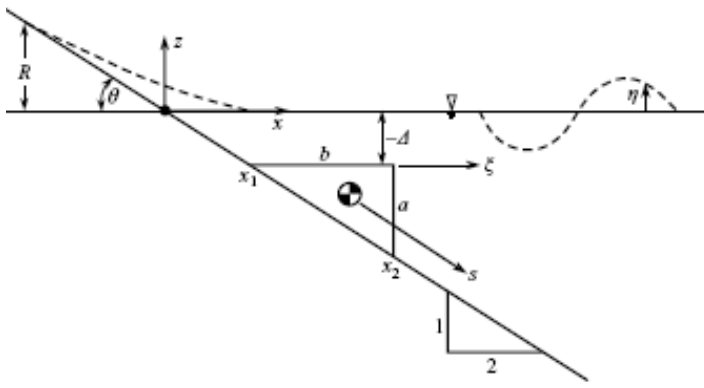
Figure 1. A schematic of the experimental setup used in the experiment at Oregon State University [14]
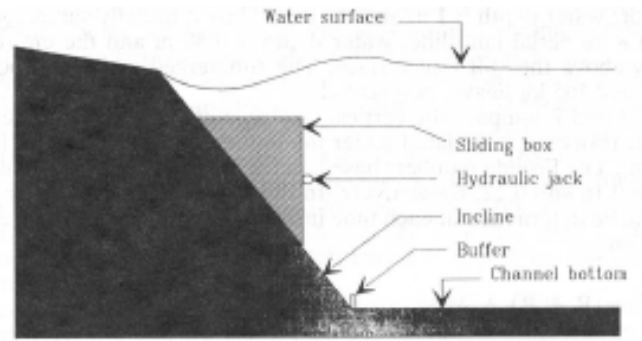


Figure 2. A schematic of the experimental setup used in the experiment by Heinrich [27]
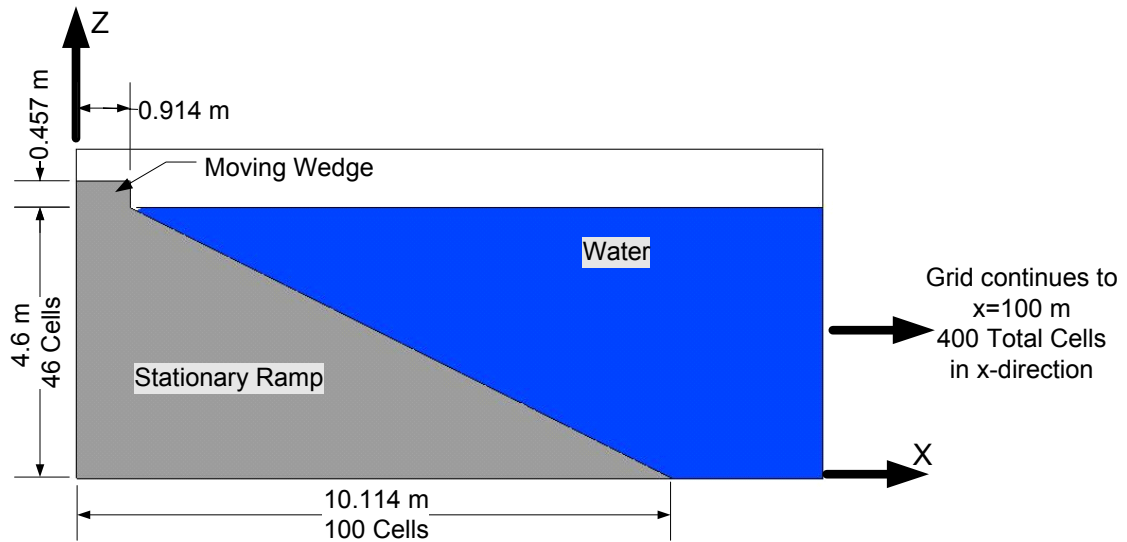


Figure 3. Flow domain and initial fluid configuration used in the simulations for the Oregon State University case [14]
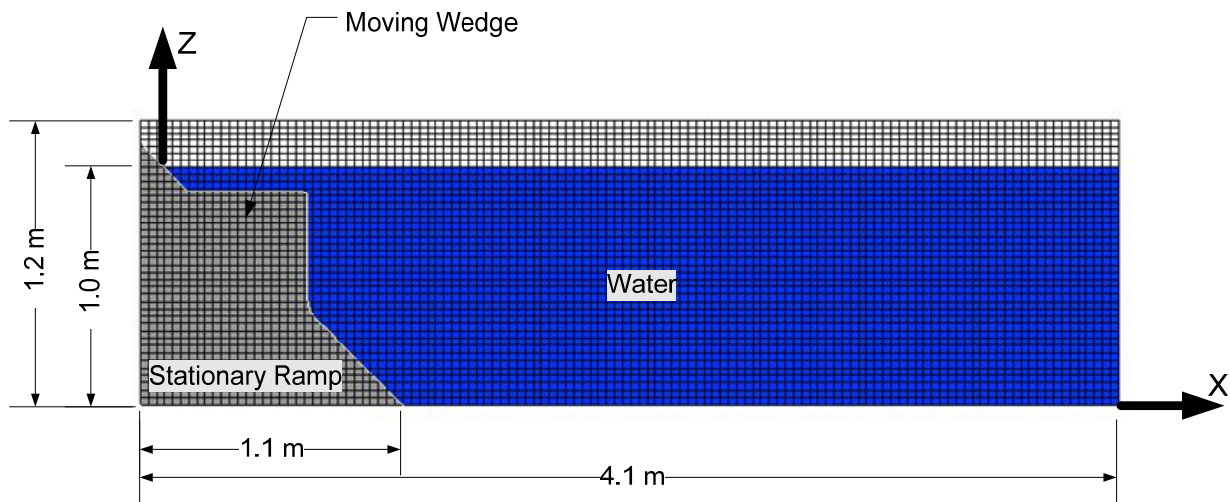


Figure 4. Flow domain and initial fluid configuration used in the simulations for the experimental data of Heinrich [27]
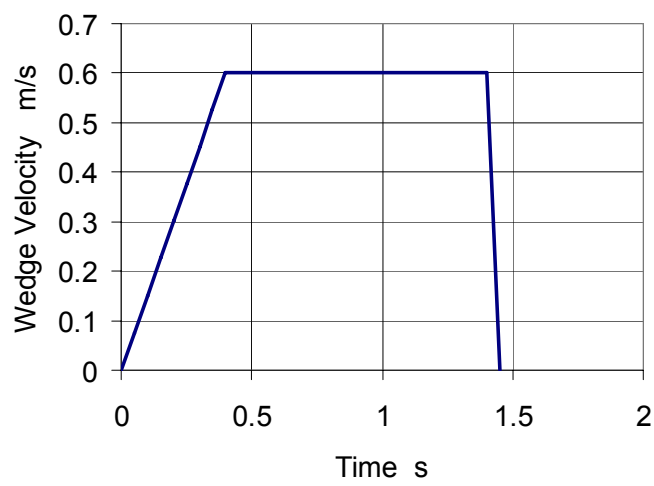
11

Figure 5 Prescribed time history of the wedge speed for the experimental data of Heinrich [27]



t=0.6 sec



t=1.2 sec
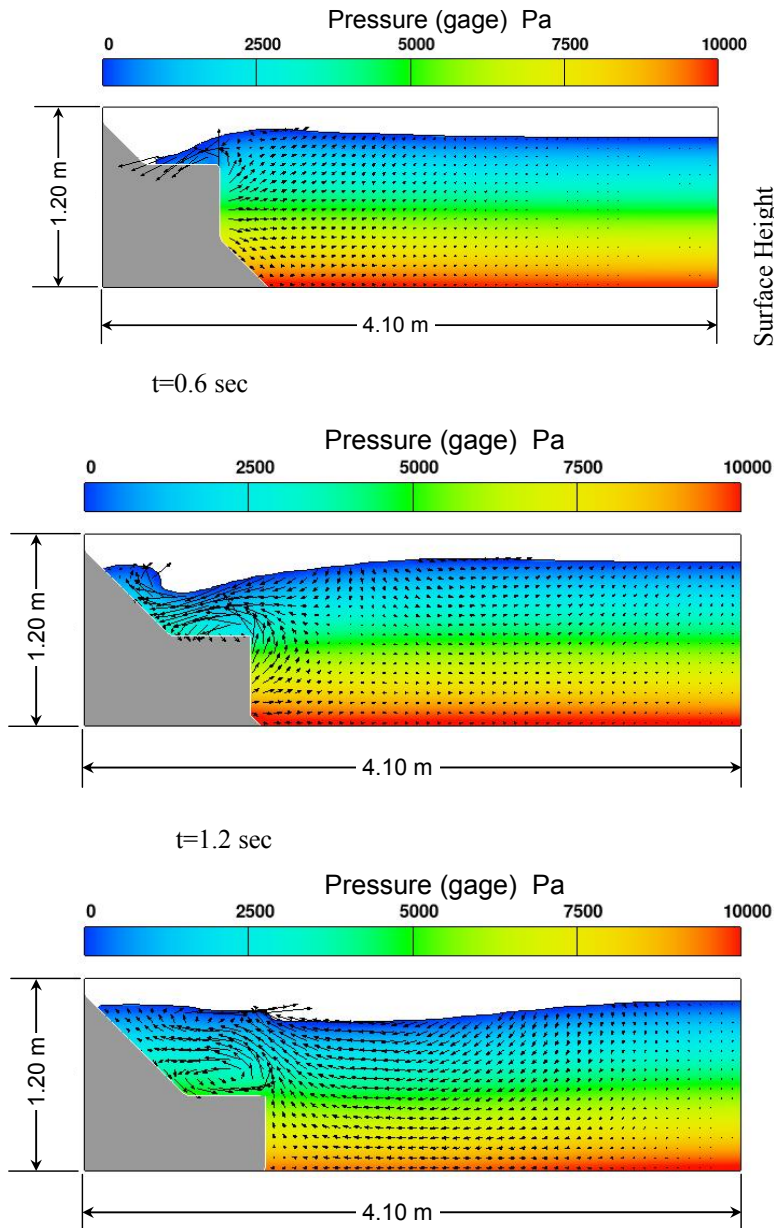


Figure 6 Fluid configurations in the simulations for the experimental data of Heinrich [27]
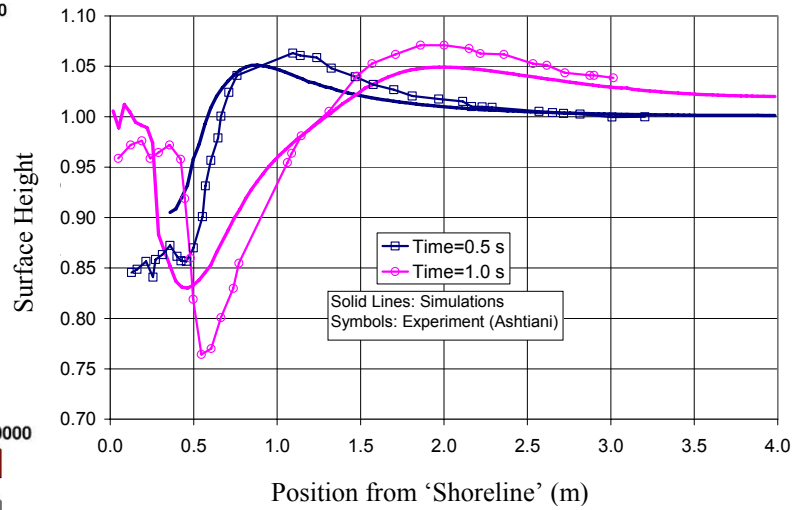


Figure 7 Water surface elevation (fluid surface profiles) at two different time instances (t=0.5 s and t=1 s)
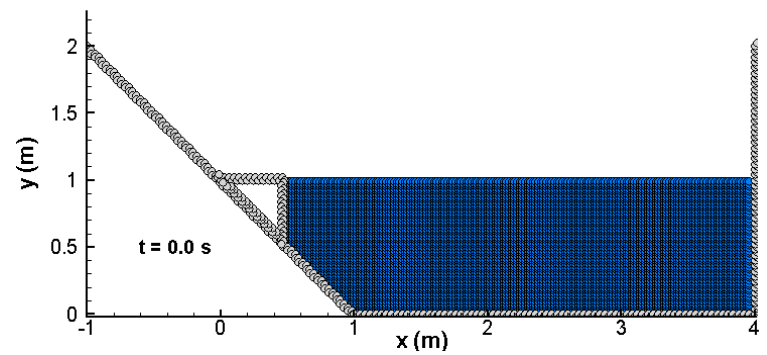


Figure 8 Initial fluid configurations in the SPH simulations for the experimental data of Heinrich [27]

11                    Copyright © 2009 by ASME
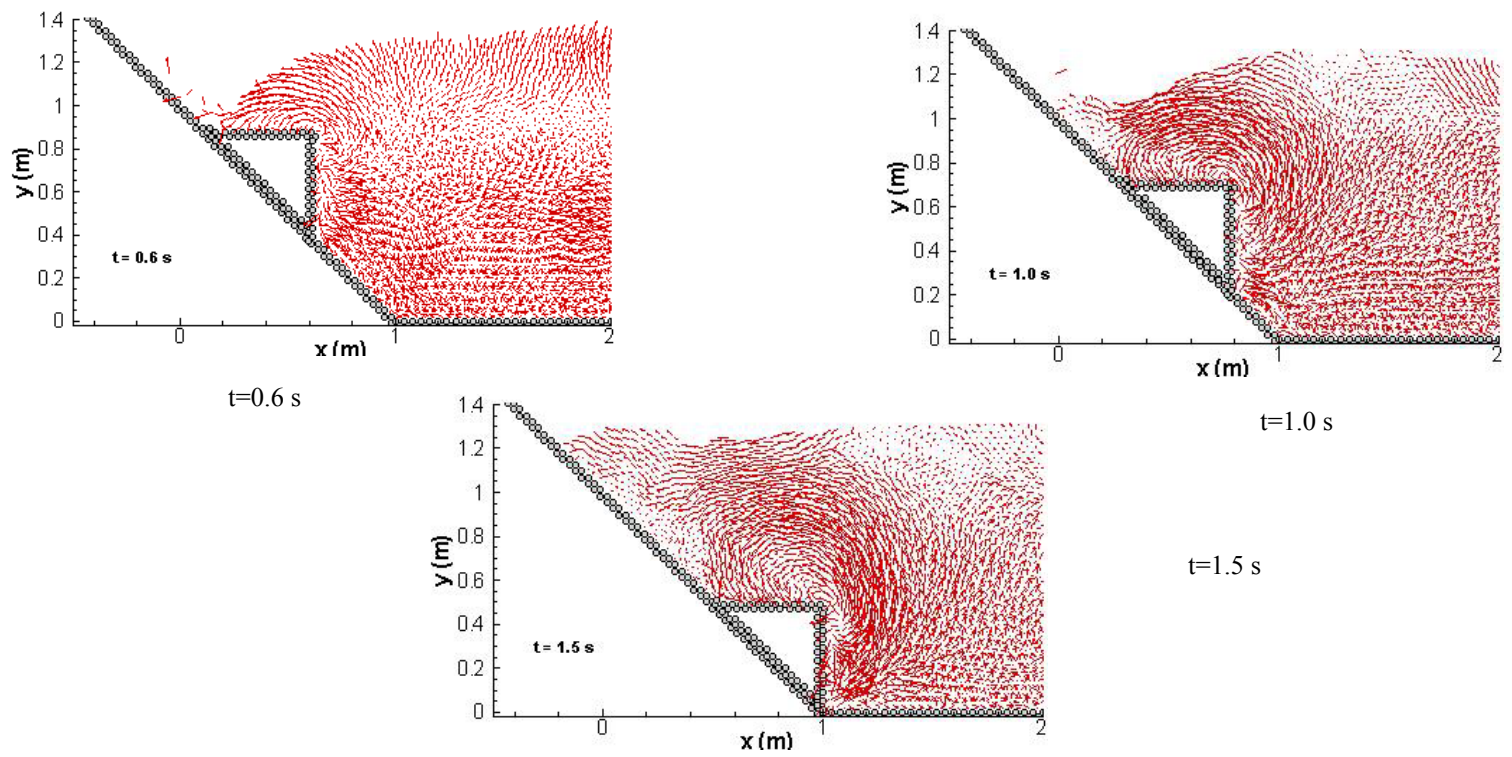
Figure 9 Water surface elevation and fluid surface profiles at different times from the SPH simulations of Heinrich [27] configuration
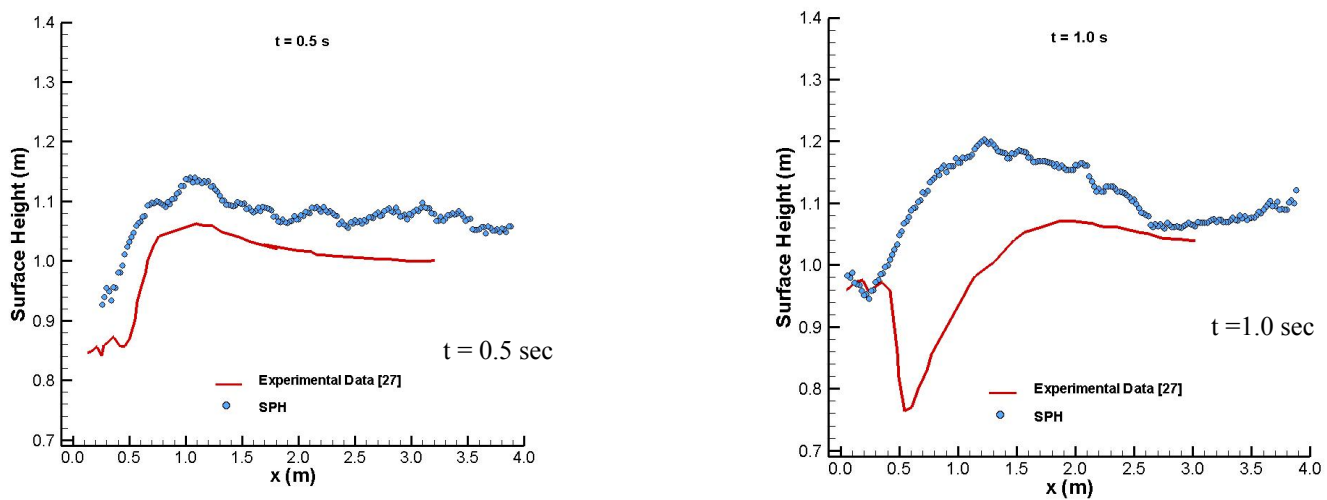


Figure 10 Comparison of water surface elevation at different times from the SPH simulations with experimental data [27]
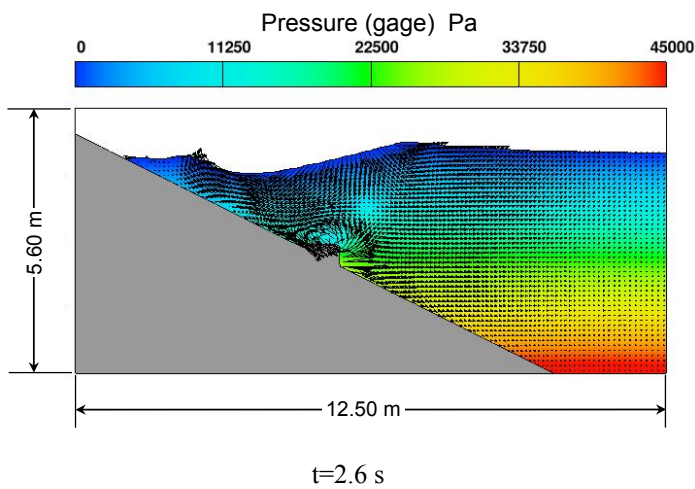


Copyright © 2009 by ASME

t=2.6 s

t=4.0 s
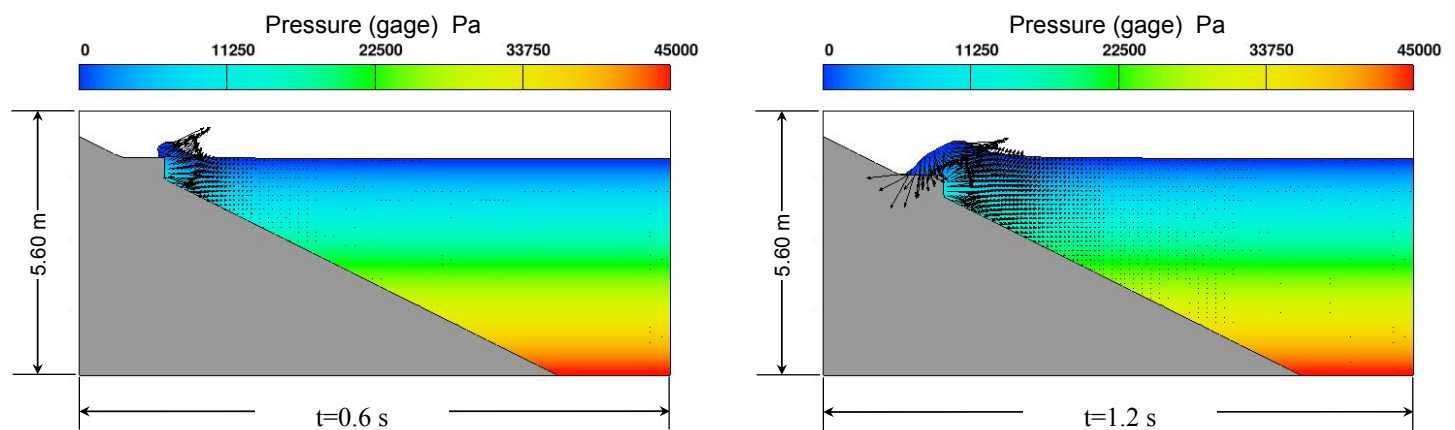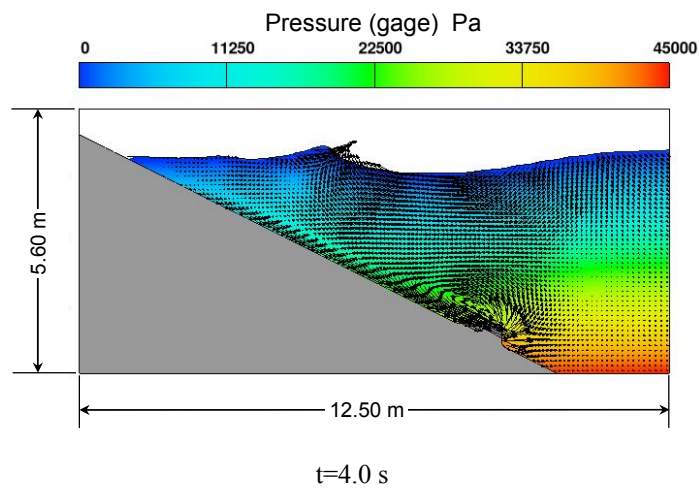
Figure 11.  Fluid configuration at different times in the Navier-Stokes simulations for the Oregon State University case [14]
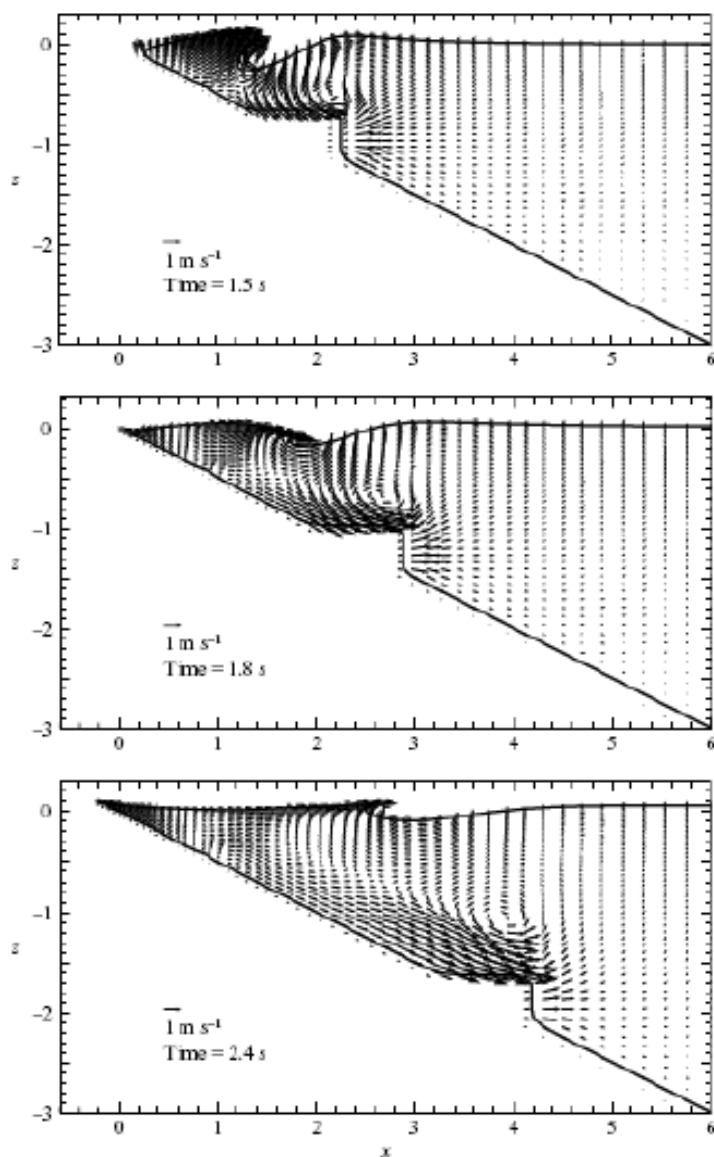


Figure 12  Snapshots of velocity vectors on the centerline vertical plane for the sliding wedge from the large eddy simulations by Liu, et al. [14]
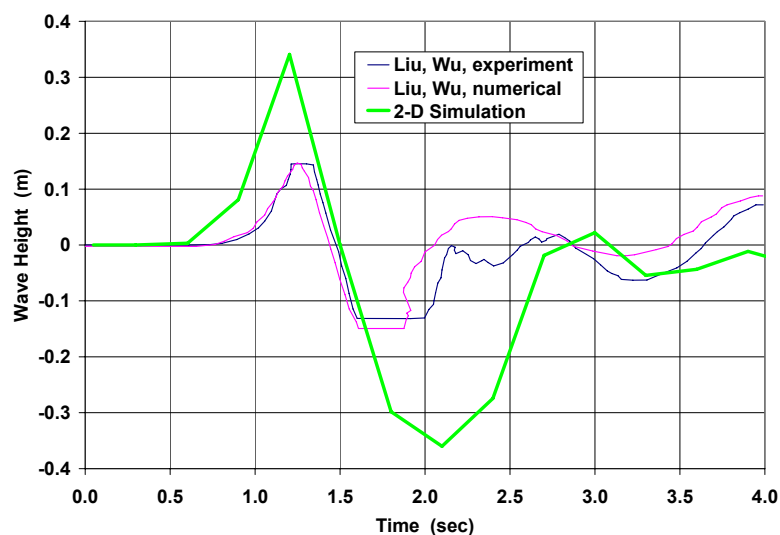


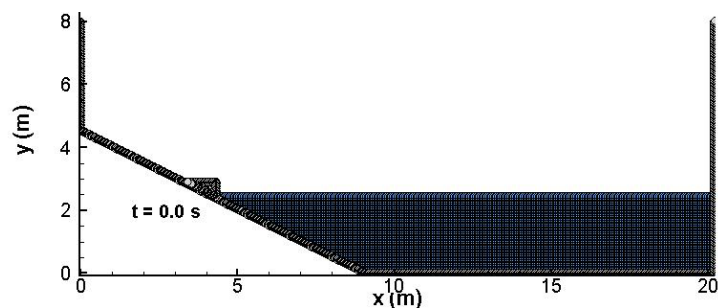Figure 13 Comparison of water height with the experimental results [14]



Figure 14 Initial fluid configurations in the SPH simulations for the configuration of Liu et al. [14]
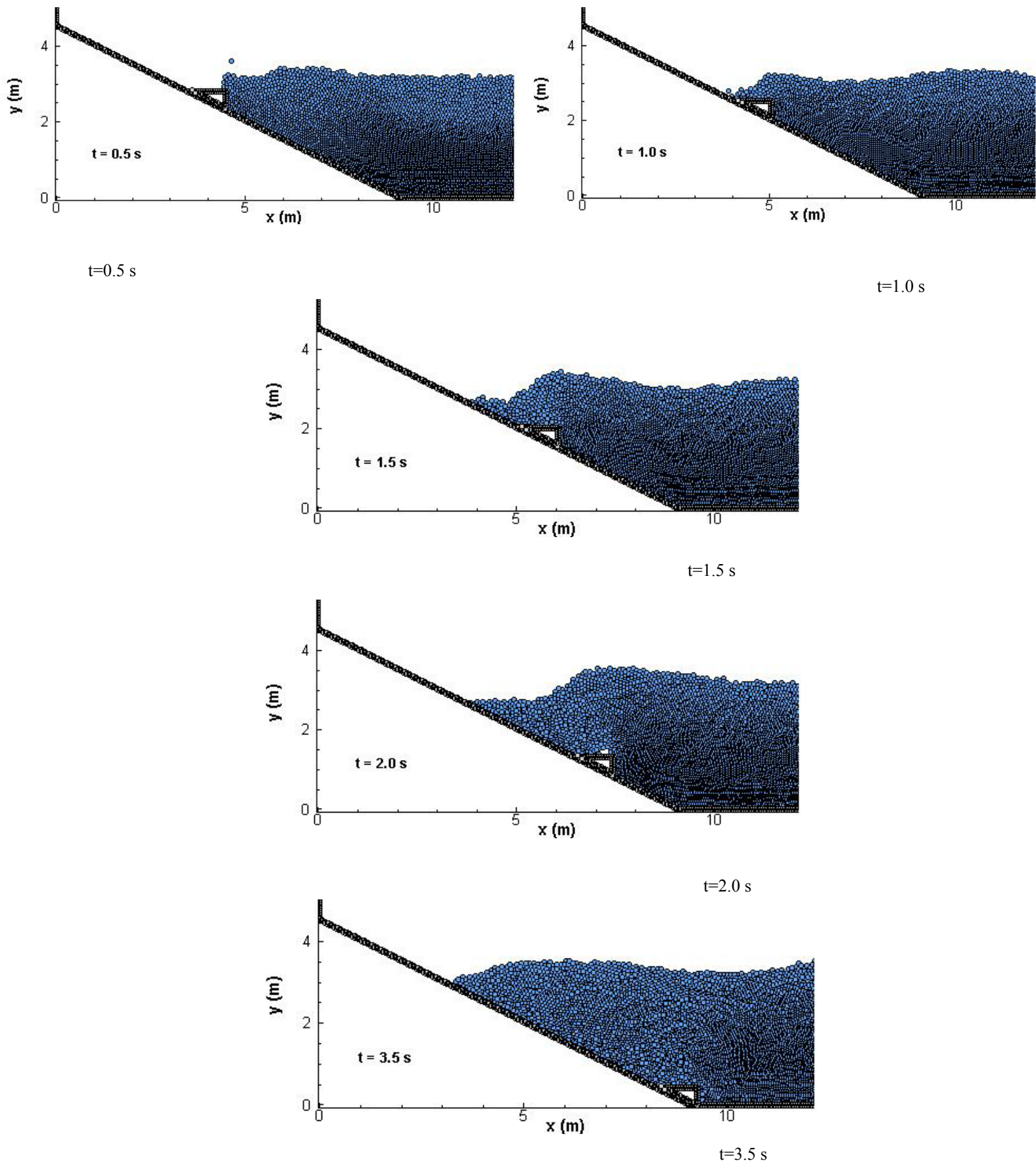
13

t=0.5 s

t=1.0 s

t=1.5 s

t=2.0 s

t=3.5 s

Figure 15.  Fluid runup at different times in the SPH simulations for the Oregon State University case [14]